New Evaluation and Test of Sidewall's Rotational Stiffness of Radial Tire

Young-woo Kim*
Department of Mechanical Engineering, Sunchon National University, Chonnam 540-742, Korea
Yongsung Kim
Graduate Student, Department of Mechanical Engineering, Sunchon National University, Chonnam 540-742, Korea

In this paper, we have revisited the estimation of the rotational stiffness of sidewall of radial tire and have suggested a new method for evaluation of the rotational stiffness. Since thicknesses, and volume fractions of the constituents of sidewall are varied depending on radial position, the equivalent shear modulus of the sidewall also depends on radial position. For the estimation of rotational stiffness of sidewall's rubber, we have divided its cross-section into sufficient numbers of small parts and have calculated the equivalent shear modulus of each part of sidewall. Using the shear moduli of divided parts, we have obtained the rotational stiffness by employing in-plane shear deformation theory. This method is expected to be a useful tool in tire design since it relates such basic variables to the global stiffness of tire. Applying the calculation method to a radial tire of P205/60R15, we have compared its rotational stiffness with experimental one.

Key Words : Radial Tire, Rotational Stiffness of Sidewall, Carcass Cord, Equivalent Shear Modulus, Netting Theory, In-Plane Shear Deformation

Nomenclature

α : Cord angle, Fig. 5
α_D : Cord angle at the belt end, Fig. 4
ϕ : Meridian angle, Fig. 5
ϕ_D : Meridian angle at belt end, Fig. 4
ψ : Rim rotational angle, Fig. 1
r, θ, z : Coordinates, Fig. 1 and Fig. 6
r_B : r-coordinate of the bead point, Fig. 4
r_B : r-coordinate of rim point, Fig. 4
r_C : r-coordinate of the turning point, Fig. 4
r_D : r-coordinate of the belt end, Fig. 4
T : Applied torque, Fig. 1

* Corresponding Author,
E-mail : kyw@sunchon.ac.kr
TEL : +82-61-760-2526; **FAX** : +82-61-750-3530
Graduate Student, Department of Mechanical Engineering, Sunchon National University, Chonnam 540-742, Korea. (Manuscript **Received** August 18, 2005; **Revised** March 17, 2006)

1. Introduction

Modern tire structures have evolved through a series of modifications of the original pneumatic rubber tire. These modifications were based on field experiences and on mostly experimental studies of tire behavior. The use of mathematical analysis to calculate tire stresses and deformations remained limited in scope for a long time because of the complexity of tire structure (Robecchi, 1973; Kennedy et al., 1982).

It is worthwhile to use a simpler tire model of "spring bedded ring model," which is consisted of the sidewall and tread including the belt structure. This simple model has been used effectively since Fiala (1954) gave an explicit formula for cornering characteristics of a running tire. It has been applied to investigations on riding comfort (Takayama et al., 1984), vibration (Tielking, 1965; Potts et al., 1977; Kamitamari et al., 1985; Huang

et al., 1987 ; Pacejka, 1981 ; Dohrmann, 1998), standing wave phenomena (Padovan, 1976 ; Chatterjee et al., 1999), contact pressure distribution (Jenkins, 1982), and rolling resistance (Stutts et al., 1992). Akasaka et al.(1984) have given an analytical method for estimating sidewall's rotational stiffness of radial tire.

In this paper, we have revisited the Akasaka's calculation of the rotational stiffness of sidewall (Akasaka et al., 1984). According to them, the rotational stiffness of the spring bedded ring model consists of two parts ; one is the stiffness due to cord tension which is caused by inflation pressure, the other is the stiffness due to the rubber compounds. However, their calculation of the latter stiffness seems to be somewhat rough or unclear in that they divided the sidewall into three spans and used shear moduli of the three. This makes the calculation a rough estimate not only because it is nearly impossible to sample accurate test specimens from the real tire due to non-uniformity of the cross-section, but also because the equivalent shear modulus is varied from point to point due to the non-uniformity of volume fractions of rubber compounds within the cross-section. This paper has suggested how to overcome the drawback by dividing the cross-section into sufficient numbers of small parts and employing an equivalent shear modulus of each part of sidewall. The equivalent shear modulus of each part is calculated by using thicknesses, material properties, and volume fractions of rubber compounds within the part under consideration. Since this method relates such variables to the rotational stiffness of sidewall, it can be utilized for determination of the appropriate values of design variables for a required stiffness in tire design. Applying the method to a radial tire of P205/60R15, we have compared its rotational stiffness with experimental one.

2. Theory

The rotational stiffness of the sidewall is defined as

$$R=\frac{T}{\psi} \tag{1}$$

when the tread is fixed as shown in Fig. 1.

Assuming that the sidewall is a composite toroidal membrane structure under inflation pressure p and considering that the sidewall is composed of fiber-reinforced laminates with rubber compound matrix as shown in Fig. 2, we can assume that they take share in the applied torque T in the manner of

$$T=T(c)+T(s) \tag{2}$$

where $T(c)$ is the torque shared by the carcass cord and $T(s)$ is the torque shared by the rubber compounds.

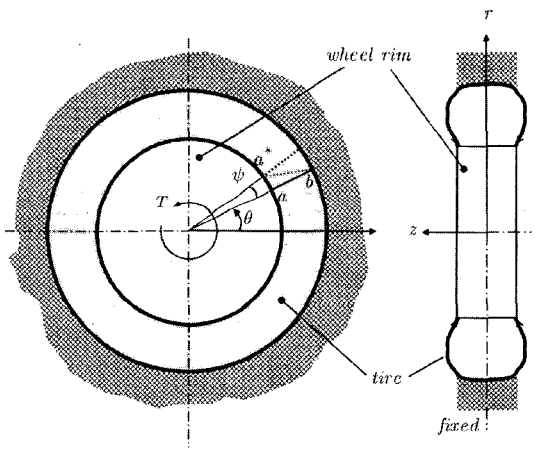

Fig. 1 Applied torque T and the rotational angle ψ ; the line $\overline{ab}$ before deformation becomes $\widehat{ab^*}$ after deformation

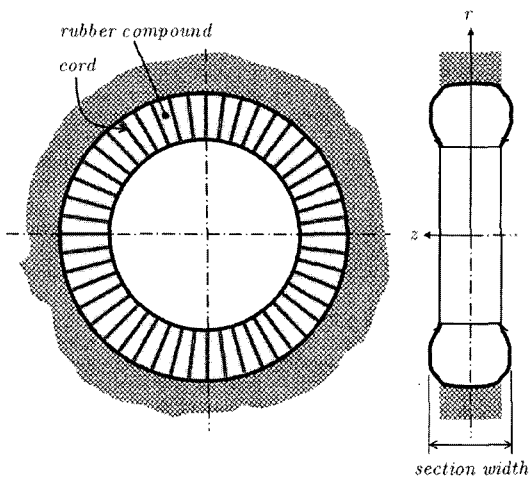

Fig. 2 Sidewall as a composite membrane structure

If the cord is inextensible, it will deform the contour of sidewall in a manner that the section width is decreased slightly as shown in Fig. 3. Therefore, $T(c)$ is expressed as

$$T(c)=2(n)(t)(r_D\cos\alpha_D) \tag{3}$$

where n is the cord end count, t is cord tension under inflation pressure p. The factor of 2 is multiplied since there are two sidewalls.

Let N denote the shear force per thickness of sidewall on the cross section at r, then $T(s)$ is expressed by

$$T(s)=2(2\pi rN)(r) \tag{4}$$

From Eqs. (1) and (2),

$$R=\frac{T(c)+T(s)}{\psi}=R(c)+R(s) \tag{5}$$

where

$$R(C)=\frac{T(c)}{\psi} \tag{6}$$

and

$$R(s)=\frac{T(s)}{\psi} \tag{7}$$

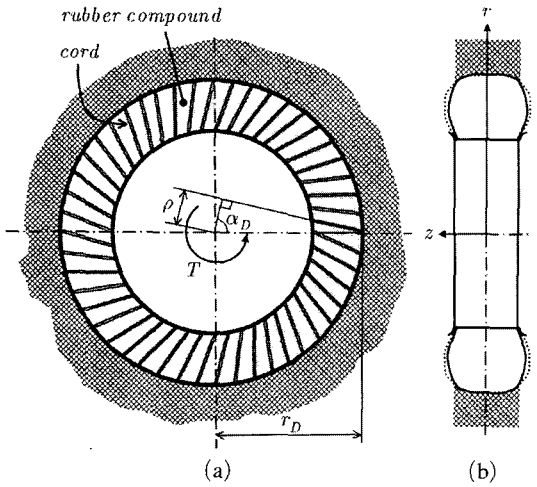

Fig. 3 Deformation of sidewall after torque loading; (a) deformation of cord and rubber compound and (b) the contour of sidewall before and after torque loading where the dotted line denotes the contour before deformation and the solid line denotes the contour after deformation

We will calculate $R(c)$ by using the netting theory and $R(s)$ by employing in-plane shear deformation theory.

2.1 Netting theory

The basic assumption of the netting theory is that the cord is inextensible and always runs along the geodesic path on the deformed toroidal surface of the sidewall. The relation between the applied torque $T(c)$ and the rotation angle ψ can be obtained by analyzing, under the basic assumption.

Assuming that the cord is laid along a geodesic path on the deformed sidewall surface, the sidewall contour can be expressed by the following equation (Day and Gehman, 1963):

$$z(r)=\int_r^{r_D}\frac{A}{\sqrt{B^2-A^2}}dr \tag{8}$$

where

$$A=(r^2-r_c^2)\sin\phi_D\frac{r\sin\alpha_D}{\sqrt{r^2-\rho^2}}$$

$$B=r_D^2-r_c^2$$

and

$$\rho=r\cos\alpha=r_D\cos\alpha_D$$

Applying Eq. (8) to the real tire of P205/60R15, we plotted the sidewall contour in Fig. 4.

In Fig. 4, we assume that the interval between

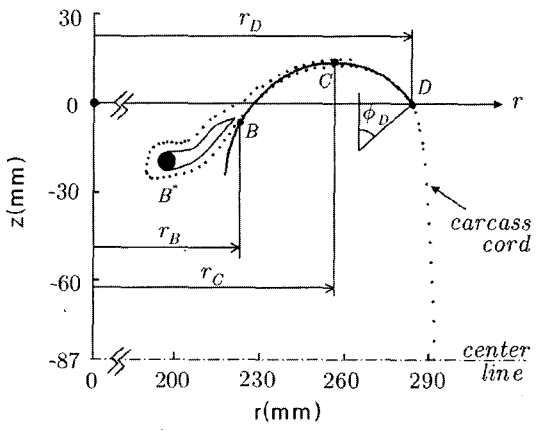

Fig. 4 Comparison between carcass cord (dotted curve) and the curve obtained by Eq. (8) (solid curve) where r_B=222 mm, r_C=256 mm, r_D=283.84 mm and ϕ_D=54°

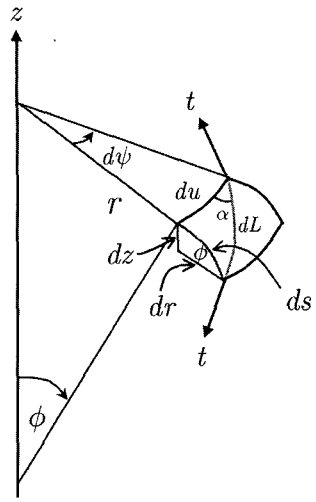

Fig. 5 Geodesic cord on a toroidal surface

the bead center B^* and the point B is firmly connected with the rigid rim, where the relative movement is entirely prevented, and the interval from B to the belt end D would be a deformable composite toroidal membrane structure under inflation pressure p.

The differential lengths and angle in Fig. 5 are given by

$$ds=\sqrt{1+\left(\frac{dz}{dr}\right)^2}dr=\frac{B}{\sqrt{B^2-A^2}}dr \tag{9}$$

$$dL=\frac{ds}{\sin\alpha}=\frac{B}{\sqrt{B^2-A^2}}\frac{r}{\sqrt{r^2-\rho^2}}dr \tag{10}$$

and

$$d\psi=\frac{du}{r}=\frac{\cot\alpha ds}{r} \tag{11}$$

Then, we have the cord length

$$L=\int_{r_B}^{r_D}\frac{B}{\sqrt{B^2-A^2}}\frac{r}{\sqrt{r^2-\rho^2}}dr \tag{12}$$

and the rotational angle

$$\psi=\int_{r_B}^{r_D}\frac{(r_D^2-r_C^2)\rho}{r\sqrt{(r_D^2-r_C^2)^2(r^2-\rho^2)-r^2(r^2-r_C^2)^2\sin^2\phi_D\sin^2\alpha_D}}dr \tag{13}$$

Since the cord tension is given by (Robecchi, 1973)

$$t=p\pi\frac{r_D^2-r_C^2}{n\sin\phi_D\sin\alpha_D} \tag{14}$$

the torque $T(c)$ in Eq. (3) is expressed as

$$T(c)=\frac{2\pi p r_D(r_D^2-r_C^2)}{\sin\phi_D}\cot\alpha_D \tag{15}$$

Since the non-linear relationship between rotational angle ψ and the torque $T(c)$ becomes apparent as ψ increases, the linear rotational stiffness $R(c)$ due to cord tension can be defined by $dT(c)/d\psi$ at $\psi=0$. Then

$$R(c)=\frac{\frac{\partial T(c)}{\partial r_C}\delta r_C+\frac{\partial T(c)}{\phi_D}\delta\phi_D+\frac{\delta T(c)}{\partial\alpha_D}\delta\alpha_D}{\frac{\partial\psi}{\partial r_C}\delta r_C+\frac{\partial\psi}{\phi_D}\delta\phi_D+\frac{\partial\psi}{\partial\alpha_D}\delta\alpha_D} \tag{16}$$

where

$$\begin{Bmatrix}\delta r_C\\ \delta\phi_D\end{Bmatrix}=\frac{1}{\frac{\partial z_B}{\partial r_C}\frac{\partial L}{\partial\phi_D}-\frac{\partial z_B}{\partial\phi_D}\frac{\partial L}{\partial\alpha_D}}\begin{pmatrix}\frac{\partial z_B}{\partial\phi_D}\frac{\partial L}{\partial\alpha_D}-\frac{\partial L}{\partial\phi_D}\frac{\partial z_B}{\partial\alpha_D}\\ \frac{\partial L}{\partial r_C}\frac{\partial z_B}{\partial\alpha_D}-\frac{\partial z_B}{\partial r_C}\frac{\partial L}{\partial\alpha_D}\end{pmatrix}\delta\alpha_D \tag{17}$$

The Eq. (17) is obtained from the fixed condition at B, $\delta z_B=0$ and the cord inextensibility, $\delta L=0$. Solving the nonlinear equation with the given initial data such as $r_C=222$ mm, $\phi_D=54°$ and $\alpha_D=\pi/2$, we can determine $R(c)=\left(\frac{dT(c)}{d\psi}\right)_{\psi=0}$. The partial derivatives involved in Eqs. (16) and (17) are calculated as follows;

$$\frac{\partial T(c)}{\partial r_C}=-\frac{4\pi p r_D r_C}{\sin\phi_D}\cot\alpha_D$$

$$\frac{\partial T(c)}{\partial\phi_D}=-\frac{2\pi p r_D(r_D^2-r_C^2)\cot\alpha_D\cos\phi_D}{\sin^2\phi_D}$$

$$\frac{\partial T(c)}{\partial\alpha_D}=-\frac{2\pi p r_D(r_D^2-r_C^2)}{\sin\phi_D\sin^2\alpha_D}$$

$$\frac{\partial\psi}{\partial r_C}=\int_{r_B}^{r_D}\frac{-2\rho r_C}{rD^{1/2}}dr+\int_{r_B}^{r_D}\frac{2\rho(r_D^2-r_C^2)r_C\{(r_D^2-r_C^2)(r^2-\rho^2)-r^2(r^2-r_D^2)\sin^2\phi_D\sin^2\alpha_D\}}{rD^{3/2}}dr$$

$$\frac{\partial \psi}{\partial \phi_D}=\int_{r_B}^{r_D}\frac{r(r_D^2-r_C^2)\rho(r^2-r_C^2)^2\sin\phi_D\cos\phi_D\sin^2\alpha_D}{D^{3/2}}dr$$

$$\frac{\partial \psi}{\partial \alpha_D}=-\int_{r_B}^{r_D}\frac{(r_D^2-r_C^2)r_D\sin\alpha_D}{rD^{1/2}}dr-\int_{r_B}^{r_D}\frac{(r_D^2-r_C^2)^3r_D^3\cos^2\alpha_D\sin\alpha_D}{rD^{3/2}}dr$$
$$+\int_{r_B}^{r_D}\frac{(r_D^2-r_C^2)r_Dr(r^2-r_C^2)^2\sin^2\phi_D\sin\alpha_D\cos^2\alpha_D}{D^{3/2}}dr$$

$$\frac{\partial z_B}{\partial r_C}=-2r_C\sin\phi_D\sin\alpha_D\times$$
$$\int_{r_B}^{r_D}\left[\frac{r}{D^{1/2}}-\frac{r(r^2-r_C^2)\{(r_D^2-r_C^2)(r^2-r_D^2\cos^2\alpha_D)-r^2(r^2-r_C^2)\sin^2\phi_D\sin^2\alpha_D\}}{D^{3/2}}\right]dr$$

$$\frac{\partial z_B}{\partial \phi_D}=\cos\phi_D\sin\alpha_D\left\{\int_{r_B}^{r_D}\frac{r(r^2-r_C^2)}{D^{1/2}}dr+\sin^2\phi_D\sin^2\alpha_D\int_{r_B}^{r_D}\frac{r^3(r^2-r_C^2)^3}{D^{3/2}}dr\right\}$$

$$\frac{\partial z_B}{\partial \alpha_D}=\sin\phi_D\cos\alpha_D\left[\int_{r_B}^{r_D}\frac{r(r^2-r_C^2)}{D^{1/2}}+\sin^2\alpha_D\int_{r_B}^{r_D}\frac{r(r^2-r_C^2)\{r^2(r^2-r_C^2)^2\sin^2\phi_D-r_D^2(r_D^2-r_C^2)^2\}}{D^{3/2}}dr\right]$$

$$\frac{\partial L}{\partial r_C}=-2r_C\int_{r_B}^{r_D}\frac{r}{D^{1/2}}dr$$
$$+2(r_D^2-r_C^2)r_C\int_{r_B}^{r_D}\frac{r\{(r_D^2-r_C^2)(r^2-r_D^2\cos^2\alpha_D)-r^2(r^2-r_C^2)\sin^2\phi_D\sin^2\alpha_D\}}{D^{3/2}}dr$$

$$\frac{\partial L}{\partial \phi_D}=(r_D^2-r_C^2)\sin\phi_D\cos\phi_D\sin^2\alpha_D\int_{r_B}^{r_D}\frac{r^3(r^2-r_C^2)^2}{D^{3/2}}dr$$

$$\frac{\partial L}{\partial \alpha_D}=-(r_D^2-r_C^2)\sin\alpha_D\cos\alpha_D\int_{r_B}^{r_D}\frac{r\{(r_D^2-r_C^2)^2r_D^2-r^2(r^2-r_C^2)^2\sin^2\phi_D\}}{D^{3/2}}dr$$

where

$$D=(r_D^2-r_C^2)^2(r^2-\rho^2)-r^2(r^2-r_C^2)^2\sin^2\phi_D\sin^2\alpha_D$$

2.2 In-plane shear deformation theory

From the assumption that the sidewall is a composite toroidal membrane structure, consider the in-plane shear deformation of the sidewall due to torque loading as shown in Fig. 6. The average shear stress at the cross-section normal to the cord line at distance r can be expressed as

$$\tau=G_{eq}\gamma \tag{18}$$

where G_{eq} denotes equivalent shear modulus of sidewall and it is expressed as

$$G_{eq}=\frac{1}{\frac{V_m}{G_m}+\frac{V_c}{G_c}} \tag{19}$$

here $V_{[..]}$ and $G_{[...]}$ are volume fraction and shear modulus of the material in brackets, respectively. The subscript "m" denotes rubber compound and "c" denotes cord, respectively.

Then the shear force per thickness ($N_{\phi\theta}$) is expressed as

$$N_{\phi\theta}=\tau h=G_{eq}\gamma h \tag{20}$$

where h is the thickness of sidewall at r as shown in Fig. 6. The torque $T(s)$ in Eq. (4) is expressed as

$$T(s)=2\times 2\pi r^2N_{\phi\theta}=4\pi r^2G_{eq}\gamma h \tag{21}$$

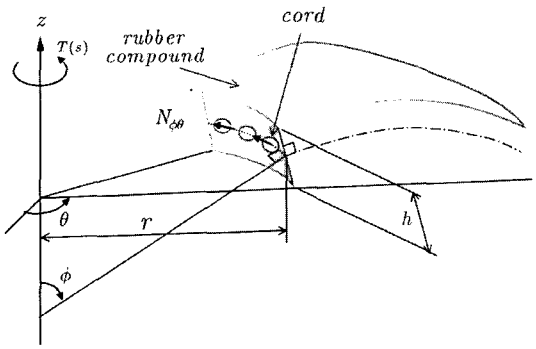

Fig. 6 Shear force per thickness on a circumferential cross-section

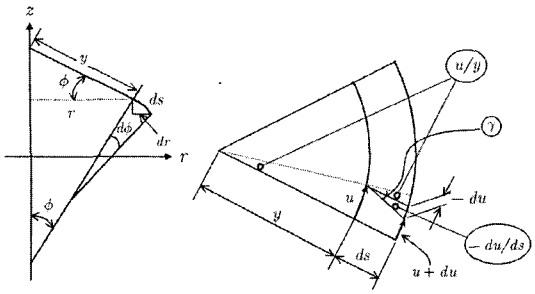

Fig. 7 Circumferential displacement u and in-plane shear strain γ

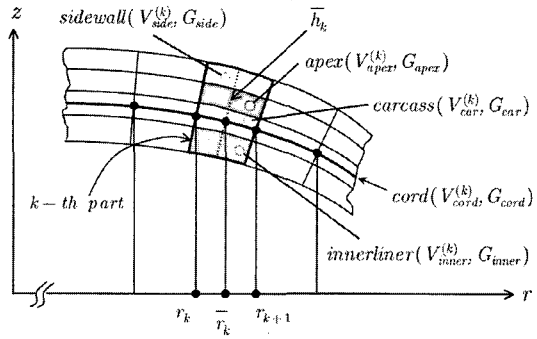

Fig. 8 Rubber compound laminates in the k-th part of the sidewall

From Eq. (21), we have

$$\gamma=\frac{T(s)}{4\pi r^2 G_{eq}h} \tag{22}$$

From the Fig. 7, the shear strain is expressed as

$$\gamma=\frac{u}{y}-\frac{du}{ds}=-\left(\frac{du}{dr}-\frac{u}{r}\right)\cos\phi \tag{23}$$

where u is a circumferential displacement.

From Eqs. (22) and (23), we have the differential equation

$$\frac{du}{dr}-\frac{u}{r}=\frac{-T(s)}{4\pi\cos\phi G_{eq}hr^2} \tag{24}$$

whose boundary conditions are

$$u_B=r_B\psi \text{ and } u_D=0 \tag{25}$$

The the solution of the Eq. (24) with boundary conditions (25) is

$$\psi=\int_{r_B}^{r_D}\frac{T(s)}{4\pi r^3\cos\phi G_{eq}h}dr \tag{26}$$

from which we obtain the rotational stiffness due to shear deformation,

$$R(s)=\frac{T(s)}{\psi}=\frac{1}{\int_{r_B}^{r_D}\frac{1}{4\pi r^3\cos\phi G_{eq}h}dr} \tag{27}$$

where $\cos\phi=\dfrac{\sqrt{B^2-A^2}}{B}$.

2.3 How to calculate G_{eq} and $R(s)$

Since G_{eq}, $\cos\phi$ and h in Eq. (27) are implicit functions of r, it is impossible to integrate Eq. (27) analytically. Consider a certain cross-section of sidewall shown in Fig. 8. Dividing the cross-section of sidewall, by using lines normal to the carcass cord line, into M parts as shown in Fig. 8, we measured the volume fractions of each rubber compound in the k-th part ($V^{(k)}_{[\cdots]}$), the radial coordinates of intersections between carcass cord line and the normal lines to the cord line r_k and r_{k+1}), and the thickness ($\bar{h}_k$) of the k-th part in the normal direction to carcass cord at $r=\bar{r}_k=(r_k+r_{k+1})/2$,

Using the volume fractions of rubber compounds, the equivalent shear modulus of the k-th part can be expressed as follows (Jones, 1975):

$$(G_{eq})_k=\frac{1}{\frac{V^{(k)}_{apex}}{G_{apex}}+\frac{V^{(k)}_{side}}{G_{side}}+\frac{V^{(k)}_{inner}}{G_{inner}}+\frac{V^{(k)}_{carcass}}{G_{carcass}}+\frac{V^{(k)}_{cord}}{G_{cord}}} \tag{28}$$

where $G_{[\cdots]}$ denotes shear moulus of the material in brackets.

Since the value of $V^{(k)}_{cord}/G_{cord}$ in the denominator is so small that it can be negligible, Eq. (28) can be written as

$$(G_{eq})_k=\frac{1}{\frac{V^{(k)}_{apex}}{G_{apex}}+\frac{V^{(k)}_{side}}{G_{side}}+\frac{V^{(k)}_{inner}}{G_{inner}}+\frac{V^{(k)}_{carcass}}{G_{carcass}}} \tag{29}$$

Assuming the rubber compound is an isotropic material, we have

$$G_{[\cdots]}=\frac{E_{[\cdots]}}{2(1+\nu_m)} \tag{30}$$

where $E_{[\cdots]}$ denotes Young' modulus of the material in the brackets and ν_m denotes Poisson's ratio of rubber compounds, which is assumed as 0.49.

Using numerical integration by the trapezoidal rule, Eq. (27) can be written as

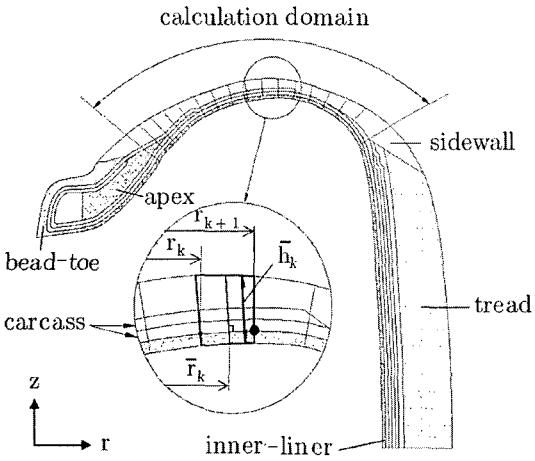

Fig. 9 Structure of sidewall and division of the calculation domain in the sidewall

$$R(s)=\frac{1}{\sum_{k=1}^{M}\frac{r_{k+1}-r_k}{4\pi(\bar{r}_k)^3(G_{eq})_k\bar{h}_k\cos\bar{\phi}_k}} \tag{31}$$

where

$$\bar{r}_k=\frac{r_k+r_{k+1}}{2}$$

$$\cos\bar{\phi}_k=\frac{\sqrt{(r_D^2-r_C^2)^2-\dfrac{((\bar{r}_k)^2-r_C^2)^2(\bar{r}_k)^2\sin^2\phi_D\sin^2\alpha_D}{(\bar{r}_k)^2-\rho^2}}}{r_D^2-r_C^2}$$

and $\bar{h}_k$ is the thickness of the k-th part in the normal direction to carcass cord at $r=\bar{r}_k$.

The division of the cross-section of sidewall into parts is shown in Fig. 9.

3. Experiments

A radial tire of P205/60R15 was used for the experimental study. Fig. 10 shows the picture of experimental apparatus equipped with a concrete block having a hole of tire size along which the tread of the tire specimen is fixed. The torque loading is applied by using UTM (universal test machine). We attached one end of wire to a point on the periphery of the rotational disk and connected the other end of wire to the grip of UTM. Pulling the wire by UTM rotates the disk and the wheel rim. At same time the UTM records the applied force (F) and displacement (δ). The applied force (F) elongates the wire and deforms

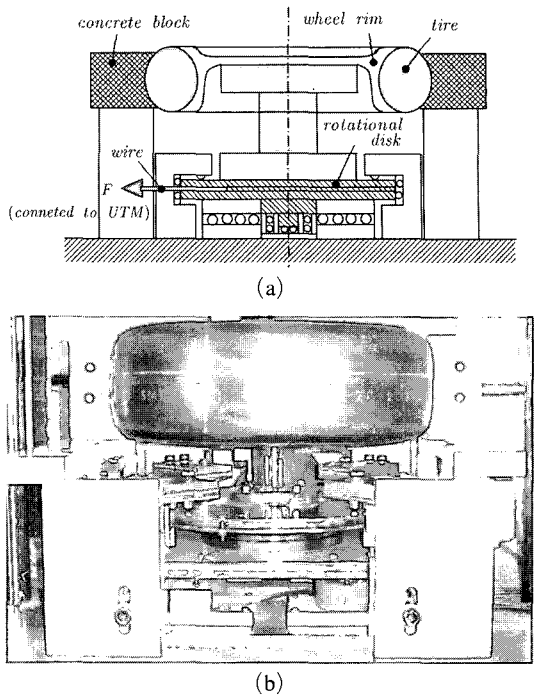

Fig. 10 (a) Schematic and (b) photo of the apparatus for measurement of rotational stiffness of sidewall

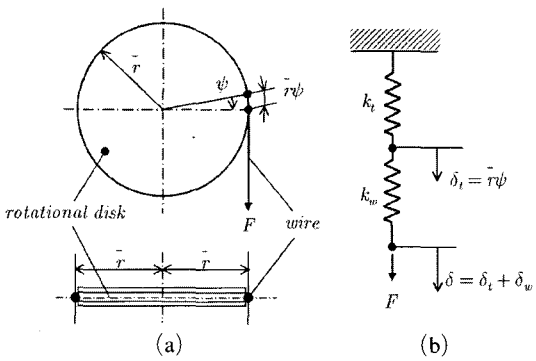

Fig. 11 (a) Rotational disk and wire, and (b) modelling of the deformation of wire-sidewall

the sidewall of tire. Thus, the displacement (δ) is consisted of the elongation of wire (δ_w) and the displacement due to the deformation of sidewall (δ_t), that is,

$$\delta=\delta_w+\delta_t \tag{32}$$

The mechanical system can be modelled by springs as shown in Fig. 11(b), where k_t is a spring con-

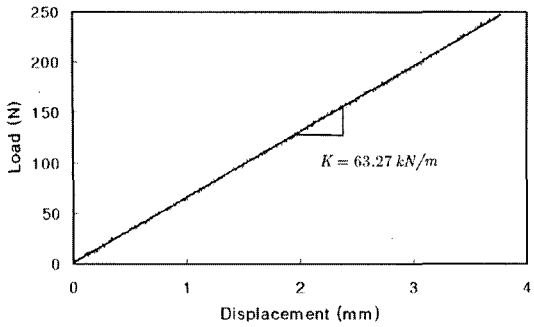

Fig. 12 Tensile test result of wire-sidewall under the inflation pressure, 2.2 kgf/cm^2

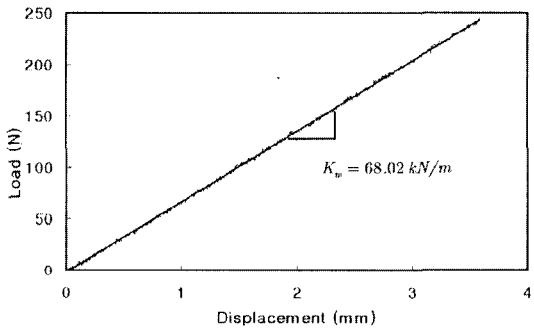

Fig. 13 Load (F)-displacement (δ_w) from tensile test of the wire

stant of sidewall and k_w is a spring constant of the wire.

The torque about the tire center due to the force (F) is given by

$$T=F\bar{r} \tag{33}$$

where $\bar{r}$ is the radius shown in Fig. 11(a). The applied torque causes angular deformation of the sidewall, ψ. The displacement along the periphery due to the angular displacement is

$$\delta_t=\bar{r}\psi \tag{34}$$

The relationship between the applied force and displacement is given by

$$F=K\delta=K_t\delta_t=k_w\delta_w \tag{35}$$

where K is the equivalent spring constant of the system and is given by

$$\frac{1}{K}=\frac{1}{k_t}+\frac{1}{k_w} \tag{36}$$

Table 1 The stiffness of wire-sidewall, K (kN/m)

Inflation pressure, p (kgf/cm^2)	Stiffness of wire-sidewall, K (kN/m)
2.5	63.52
2.4	63.40
2.2	63.27
2.0	63.14
1.75	62.93
1.50	62.74
1.25	62.26
1.00	61.99
0.75	61.56
0.50	61.06

From Eqs. (32) and (34), we have

$$\psi=\frac{\delta-\delta_w}{\bar{r}} \tag{37}$$

From Eqs. (34) and (37), the rotational stiffness of sidewall is expressed by

$$R=\frac{T}{\psi}=\frac{F(\bar{r})^2}{\delta-\delta_w} \tag{38}$$

Eq. (38) is rewritten, by using Eq. (35), as

$$R=\frac{Kk_w}{k_w-K}(\bar{r})^2 \tag{39}$$

where the spring constant K can be measured from the rotational test, and the constant k_w from a separate tensile test of wire. The radius, $\bar{r}$ can be also obtained from the apparatus. Then, we can calculate the rotational stiffness of sidewall by using Eq. (39). The test results for the spring constants K and k_w are shown in Figs. 12-13 and Table 1.

4. Results and Discussion

Young's modulus of each rubber compound is obtained from the tensile tests of specimens, which are sampled from real tire (Kim et al., 2003). All the necessary geometrical data including volume fractions can be obtained directly from the geometry of tire. Then, we can calculate equivalent shear modulus of each part of the sidewall by using Eqs. (29) and (30), and the rotational stiffness $R(s)$ by using Eq. (31). The values of $R(s)$ in

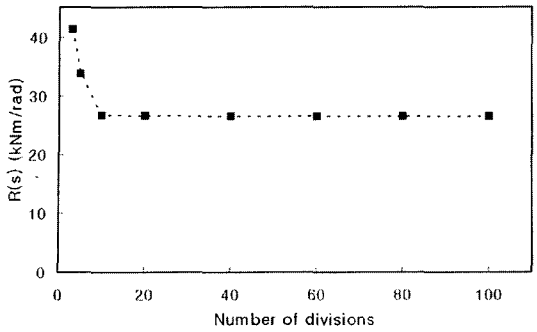

Fig. 14 Rotational stiffness of the sidewall due to rubber compound versus number of divisions

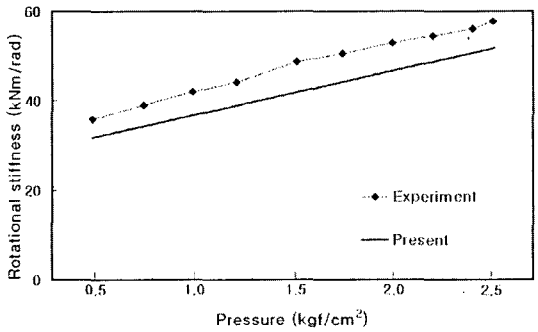

Fig. 15 Rotational stiffness of sidewall of the radial tire

terms of the number of divisions are plotted in Fig. 14, which shows that the value of converges to a certain value as the number of divisions increases. This is because refined discretization calculates the geometry of sidewall and the equivalent shear modulus precisely at each part.

For the calculation domain divided into 100 parts, the total rotational stiffness $R=R(c)+R(s)$ in terms of inflation pressure p is plotted in Fig. 15 with experimental ones and their values are compared in Table 2. Fig. 15 shows that there is some difference between theoretical prediction and experimental values.

The main reasons of the discrepancy may be originated from the following facts. Because the specimens of rubber sheets are so tricky to separate from real tire without any flaws, their Young's moduli might be estimated lower than the values of real ones (Kim et al., 2003). Secondly, the sidewall contour given by Eq. (8) cannot describe the

Table 2 Comparison of the rotational stiffness in Fig. 15

Inflation pressure, p (kgf/cm^2)	Rotational stiffness, R (kNm/rad)	
	Experiment	Present
2.50	57.7	51.8
2.40	56.1	50.7
2.20	54.4	48.6
2.00	52.9	46.7
1.75	50.5	44.3
1.50	48.6	41.7
1.25	44.2	38.8
1.00	42.0	36.7
0.75	39.0	34.3
0.50	35.8	31.8

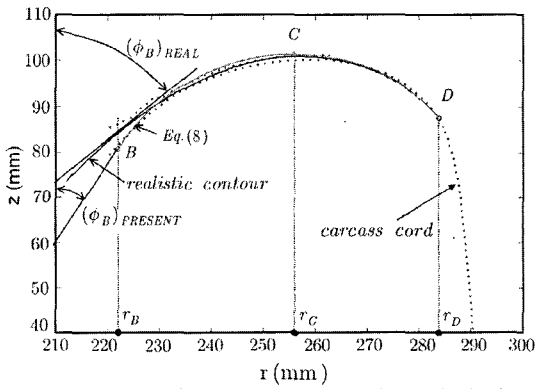

Fig. 16 Comparison between the theoretical sidewall contour obtained by Eq. (8) and a realistic contour

real contour accurately near the point B as shown in Fig. 16, which causes the value of cos ϕ in Eq. (27) to be estimated higher and the rubber stiffness $(R(s))$ to be lower than real one. Additionally, the theoretical contour gives longer cord length (L) than the real one due to the same reason, which causes the cord stiffness $(R(c))$ to be evaluated lower than real value. Therefore, the theoretical sidewall contour near the point B is the one of main reasons why the present results are lower than the experimental ones. It is required to devise a new accurate sidewall contour to reduce the difference between theoretical prediction and experimental values of rotational stiff-

ness of sidewall.

5. Conclusions

This paper has considered the calculation of sidewall's rotational stiffness of radial tire, which is consisted of cord stiffness and rubber compound stiffness. Focusing on the calculation of the stiffness of rubber compound, a new calculation method is suggested, which employs an equivalent shear modulus. Since the equivalent shear modulus is different from point to point due to the geometric non-uniformity, we divide the cross-section into sufficient number of parts and calculate the equivalent shear modulus of each part by using the shear moduli and volume fractions of rubber compounds of the part. The present method provides clearer way of estimation of shear modulus of sidewall than the conventional one, on which was mentioned in Introduction. Moreover, the present method relates the material properties, volume fractions and thicknesses of rubber compounds to the rotational stiffness, it can be used as a practical tool for a design of tire. But there is still some difference between the present prediction and experimental values of rotational stiffness, which may be arisen from the discrepancy between theoretical sidewall contour and real contour of sidewall and further research on sidewall contour is required.

References

Akasaka, T., Yamazaki, S. and Asano, K., 1984, "An Approximate Evaluation of Rotational Stiffness of Radial Tire," *Transactions of JSCM*, Vol. 10, No. 1, pp. 24~31.

Chatterjee, A., Cusumano J. P. and Zolock, J. D., 1999, "On Contact-Induced Standing Waves in Rotating Tires: Experiment and Theory," *Journal of Sound and Vibration*, Vol. 227, No. 5, pp. 1049~1081.

Clark, S. K., 1965, "The Rolling Tire under Load," SAE 650493.

Day, R. B. and Gehman, S. D., 1963, "Theory for the Meridian Section of Inflated Cord Tire," *Rubber Chemistry and Technology*, Vol. 36, No. 1, pp. 11~27.

Dohrmann, C. R., 1998, "Dynamics of a Tire-Wheel-Suspension Assembly," *Journal of Sound and Vibration*, Vol. 205, No. 5, pp. 627~642.

Fiala, E., 1954, "Seitenkraft am rollendem Luftreifen," *VDI*, Vol. 96, pp. 937~979.

Frank, F., 1965, "Grundlagen zur Berechnung der Seitenfuhrungs-Kennlinien von Luftreifen," *Kautsh. Gummi.*, Vol. 18, No. 8, pp. 515~533.

Huang, S. C. and Soedel, W., 1987, "Effect of Coriolis Acceleration on the Free and Forced In-plane Vibrations of Rotating Rings on Elastic Foundation," *Journal of Sound and Vibration*, Vol. 115, No. 2, pp. 253~274.

Jenkins, J., 1982, "The Circumferential Contact Problem for the Belted Radial Passenger Car Tire," *Vehicle System Dynamics*, Vol. 11, pp. 325~343.

Jones, R. M., 1975, *Mechanics of Composite Materials*, McGraw-Hill Book Company.

Kamitamari, T. and Sakai, H., 1985, "A Study on Radial Tire Vibration," SAE 852185, pp. 153~158.

Kennedy, R. H., Patel, H. P. and McMinn, M. S., 1982, "Radial Truck Tire Inflation Analysis: Theory and Experiment," *Rubber Chemistry and Technology*, Vol. 54, pp. 751~766.

Kim, Yong-woo and Kim, J. G., 2003, "Calculation of Sidewall Lateral Stiffness of a Radial Tire Using Material Properties of Rubber Compounds," *Transactions of KSME*, Vol. 27, No. 10, pp. 1667~1675

Pacejka, H., 1981, "Tire In-plane Dynamics," in Mechanics of Pneumatic Tires edited by Clark, S. K., pp. 726~784.

Padovan, J., 1976, "On Viscoelasticity and Stand Waves in Tires," *Tire Science and Technology*, Vol. 4, No. 4, p. 233.

Potts, G. R., Bell, C. A., Charek, L. T. and Roy, T. K., 1977, "Tire Vibrations," *Tire Science and Technology*, Vol. 5, No. 4, pp. 202~225.

Robecchi, E. and Amichi, L., 1973, "Mechanics of the Inflated Tire," *Tire Science and Technology*, Vol. 1, No. 3, pp. 290~345.

Stutts, D. S. and Soedel, W., 1992, "A Simplified Dynamic Model of the Effect of Internal Damping on the Rolling Resistance in Pneumatic Tires," *Journal of Sound and Vibration*, Vol. 155,

No. 1, pp. 153~164.

Takayama, M. and Yamagishi, K., 1984, "Simulation Model for Tire Vibration," *Tire Science and Technology*, Vol. 11, No. 1, pp. 38~49.

Tielking, J. T., 1965, "Plane Vibration Characteristics of a Pneumatic Tire Model," SAE 650492.